Imprints of log-periodicity in thermoacoustic systems close to lean blowout

Ankan Banerjee [1,*] Induja Pavithran [1,2,†] and R. I. Sujith [1,‡]

[1]*Department of Aerospace Engineering, Indian Institute of Technology Madras, Chennai 600036, India*
[2]*Department of Physics, Indian Institute of Technology Madras, Chennai 600036, India*

In the context of statistical physics, critical phenomena are accompanied by power laws having a singularity at the critical point where a sudden change in the state of the system occurs. In this work we show that lean blowout (LBO) in a turbulent thermoacoustic system is accompanied by a power law leading to finite-time singularity. As a crucial discovery of the system dynamics approaching LBO, we unravel the existence of the discrete scale invariance (DSI). In this context, we identify the presence of log-periodic oscillations in the temporal evolution of the amplitude of the dominant mode of low-frequency oscillations (A_f) existing in pressure fluctuations preceding LBO. The presence of DSI indicates the recursive development of blowout. Additionally, we find that A_f shows a faster-than-exponential growth and becomes singular when blowout occurs. We then present a model that depicts the evolution of A_f based on log-periodic corrections to the power law associated with its growth. Using the model, we find that blowouts can be predicted even several seconds earlier. The predicted time of LBO is in good agreement with the actual time of occurrence of LBO obtained from the experiment.

I. INTRODUCTION

Lean premixed combustion is one of the most sought-after technologies in gas turbine engines to satisfy the stringent emission norms of oxides of nitrogen [1]. The lean fuel-air mixture results in a significant reduction of the flame temperature inside the combustor near the reactant flame due to the presence of excess air. However, such lean conditions make an engine susceptible to a lean-flame blowout. Lean-flame blowout continues to be detrimental to the operation of modern gas turbine combustors in the power-production and aviation industries [2]. Blowout is the state when the flame fails to stabilize inside the combustor and gets blown out due to the reduced flame speed in comparison to the high flow rates of incoming reactants [3,4]. In power plants based on gas turbine engines, a blowout can lead to unplanned power outages and increased operational costs [5]. Both military and commercial aircraft engines are also susceptible to blowout during lean operation and sudden changes in throttle settings [6]. Therefore, precursors to blowout are desired to avoid an unplanned shutdown of engines in aircraft and power plants.

In order to understand the physical mechanism behind the occurrence of a blowout, a number of studies have analyzed the flame dynamics prior to its occurrence for different combustors and different flame-holding mechanisms [5,7–11]. Nair and Lieuwen [5,7] analyzed flame dynamics in a turbulent premixed combustor near blowout. They characterized blowout as a consequence of two phenomena: the emergence of localized flame extinction regions or flame holes followed by the violent flapping of the flame front or collective extinction of flames. The amplitude of acoustic oscillations increases due to such flame behavior. As the system approached blowout, they observed bursts in the amplitude of the acoustic pressure field. These bursts correspond to the extinction and reignition of flames. Later, Chaudhuri *et al.* [9] investigated the interaction between flame fronts and shear layer vortices prior to blowout in a turbulent premixed combustor with a bluff-body stabilized flame and showed that the interaction leads to local extinction of flames or generation of local (smaller) flame holes. The number of flame holes and the frequency of their appearance increase as the system approaches blowout. The collective behavior of smaller flame holes leads to the formation of a global flame hole that causes blowout. The formation of flame holes that are localized in space can be considered as an intermediate state to blowout. Such intermediate states have been used to control blowout and provide warning signals [12]. Several other phenomena, such as earthquakes and stock market crashes, are found to be preceded by similar small-scale precursory events. Studies have shown that large earthquakes [13] or stock market crashes [14] are forms of self-organized criticality and they occur as a scaling-up process of its earlier precursory events. The hierarchical dynamics underlying the precursory events were utilized to predict the corresponding critical phenomena based on the property of scale invariance [15].

The property of scale invariance means that the law governing a physical variable of a system remains invariant under the change of a scale (in length, time, energy, or some other variables) by some common factor. The scale-invariance property exists in the close vicinity of a critical point. A physical variable of the system showing such a property follows a power law with a real exponent in a local neighborhood (the so-called asymptotic critical region) of the critical point [16]. The variable is said to have the continuous scale-invariance property if the exponent of the power law is real. Moreover,

*ankan1090@gmail.com
†indujap2013@gmail.com
‡sujith@iitm.ac.in

the variable becomes singular at the critical point. In other words, the scale-invariance property ceases to exist beyond the critical point following a singularity there [16].

Although the continuous scale-invariance property can explain a transition occurring at the critical point, it has a limited scope in detecting precursory signals outside the asymptotic critical region. This limitation has been overcome by extending the exponent in the power law from a real-valued exponent to a complex-valued one. Complex-valued exponents are associated with discrete scale invariance and result in log-periodic oscillations to the scaling law (a detailed discussion is given in Sec. II). A power law decorated with the log-periodic correction is called a log-periodic power law (LPPL) [17]. A LPPL has successfully predicted upcoming transitions in several natural complex systems such as earthquakes [18] and icequakes [19] as well as in complex human-made systems such as rupture stresses from acoustic emissions [20], stock market crashes [14,21], and credit risk estimation [22], to name a few. The strength of the LPPL formulation is that it can predict an impending critical transition by detecting its implicit precursory phenomena, which are not identified by pure power-law formulation associated with continuous scale invariance in the critical region.

Detection of precursory signals to an impending blowout for providing efficient early warnings is highly desirable so that a combustor can be operated at leaner conditions without risking blowout. Thermoacoustic systems possess inherent complexity due to the nonlinear interaction between their subsystems, namely, the acoustic field, the turbulent hydrodynamic field, and the flame [23–25]. The complexity of the system intrigues researchers to investigate its dynamical behaviors, which in turn can help identify precursors to an impending blowout. Subjects such as nonlinear dynamics [26], complex systems theory [27], and pattern formation [28] have been utilized significantly in this regard.

Gotoda *et al.* used tools from nonlinear dynamics to analyze the system behavior prior to lean blowout [29–31]. The signature of self-affine structures [30] in the dynamics near lean blowout (LBO) and the translational error [31] were used as precursors to detect LBO. Mukhopadhyay *et al.* [32] proposed a precursor for LBO based on symbolic time series analysis. Multifractal characteristics of pressure fluctuations quantified by the Hurst exponent have been used as early warning signals to impending thermoacoustic instability and LBO [33,34]. Recurrence quantification analysis is another technique providing precursor measures that show distinctive signatures toward LBO [35,36]. Recently, Bhattacharya *et al.* [37] proposed a fast-Fourier-transform–based single scalar-valued measure to detect different operational regimes, namely, stable operation, thermoacoustic instability, and LBO based on the time series of acoustic pressure. Detailed discussions about the mechanism of LBO, its precursors, and control are summed up well in the review articles in [38,39].

In earlier experiments [5,7–9,11,12,34], warnings of an impending blowout and its control were dependent on user-defined threshold values of an underlying property of the associated system. Such threshold values are system dependent and act as a constraint in reaching a leaner fuel-air ratio. Moreover, the control parameter, the fuel-air ratio, was changed in a quasistatic manner and the system was

let to stabilize for each control parameter. In other words, those systems were treated as autonomous. However, real-life combustion systems are mostly nonautonomous. The control parameter constantly changes at a finite rate, which makes the analysis of the system much more challenging than an autonomous one. Therefore, in the case of a nonautonomous thermoacoustic system, it would be fascinating to investigate whether there are potential precursory signals for predicting LBO. Additionally, rather than any threshold-dependent methods, prediction of the time to LBO will be more convenient in nonautonomous systems for circumventing LBO. In the present work, we attempt to address these issues by interpreting the onset of LBO as a critical point. We then use the LPPL formulation to predict the time to LBO several seconds in advance.

II. LOG-PERIODICITY IN DISCRETE SCALE INVARIANCE

In Euclidean geometry, the dimension of a system or the number of independent vectors (or bases) representing the system is a positive integer. Mandelbrot generalized the concept of Euclidean geometry by introducing the concept of fractals, which are 'sets consisting of parts similar to the whole' [40]. Systems with fractals are said to have noninteger dimensions. Systems having noninteger dimensions possess the property of scale invariance, which is represented by the equation

$$F(x) = \mu F(\lambda x), \tag{1}$$

where x is a variable representing a scale of length, time, energy, etc. (mathematically x generates a scale), λ is a nonzero number known as the scale factor, and μ is a function of λ. Both λ and μ are real numbers and F is a function associated with a physical variable of the system [or x is a measuring variable and $F(x)$ is a measured variable]. A power law expressed as

$$F(x) = Cx^{\alpha}, \tag{2}$$

$\alpha = -\frac{\log \mu}{\log \lambda}$, is a solution to Eq. (1). Note that α in this power law gives the fractal dimension. In the case of continuous-scale invariance, α is real. The scale invariance is called continuous since λ can be any arbitrary real number. The scale-invariance property exists in an abundance of natural phenomena showing fractals, criticality, or self-organized criticality [41].

If the arbitrariness of scale factors is constrained in such a way that the scale factors are determined by a unique nonzero real number λ and belong only to the set $S = \{\lambda^i : i \text{ is an integer}, \lambda \neq 0\}$, then the scale-invariance property (1) is said to be the discrete scale invariance (DSI). In other words, the scale-invariance property holds if the scale factors are in geometric progression in λ and appears periodically at each scale factor that belongs to S. Note that the unique value of λ is system dependent. The continuous change of the variable x in the case of DSI gives the power-law solution to Eq. (1) of the form

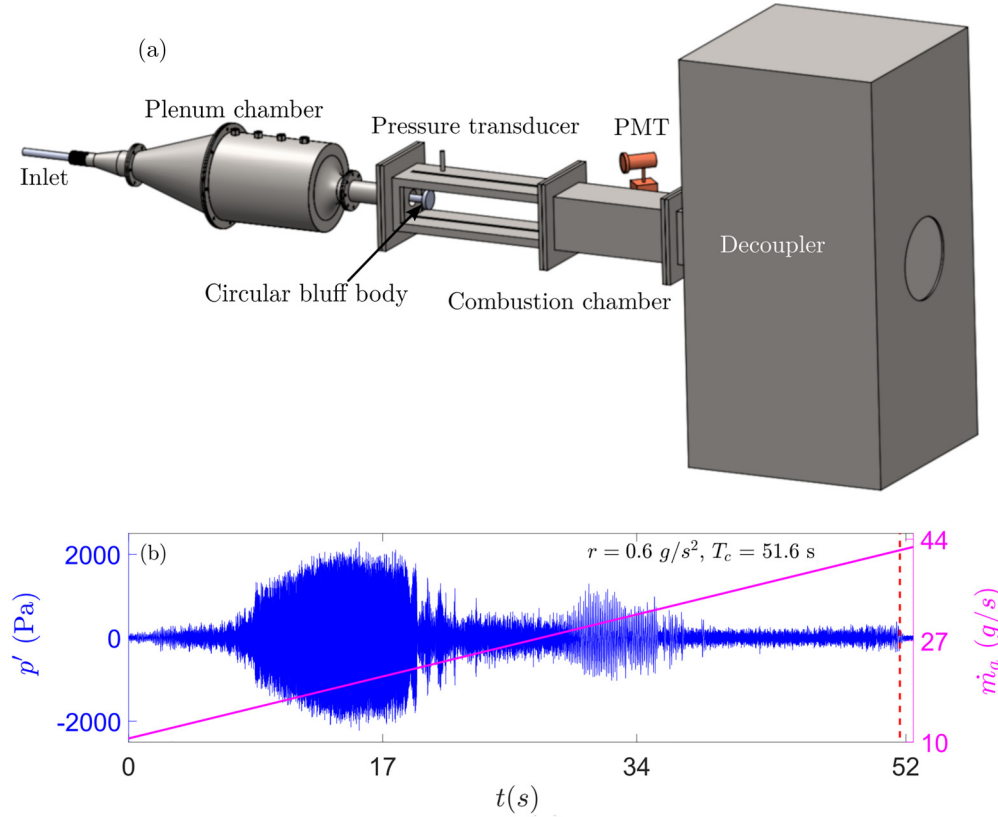$$F(x) = Cx^{\alpha} P\left(\frac{\log x}{\log \lambda}\right). \tag{3}$$

FIG. 1. (a) Schematic of the turbulent combustor used in the present study. Pressure fluctuations are measured using a piezoelectric transducer. The design of the combustor was adapted from the work of Komarek and Polifke [44]. (b) Temporal variation of the mass flow rate of air [magenta (light gray) solid line] together with the time series of pressure fluctuations [blue (black) solid curve] for the rate of change of air flow rate $a = 0.6 \, g/s^2$. The occurrence of blowout is indicated by the red (dark gray) dashed line.

By expanding the periodic term $P(\frac{\log x}{\log \lambda})$ into a Fourier series, we get

$$
\begin{aligned}
F(x) &= Cx^\alpha \sum A_n \exp\left(i2n\pi \frac{\log x}{\log \lambda} \right) \\
&= C \sum A_n x^\alpha x^{i(2n\pi/\log \lambda)} \\
&= C \sum A_n x^{\alpha + in\omega},
\end{aligned}
\tag{4}
$$

where $\omega = 2\pi/\log \lambda$. Therefore, DSI leads to a complex fractal dimension $\alpha + in\omega$. Moreover, it can be shown that the log-periodic oscillation stems from the imaginary part ($n\omega$) of complex fractal dimensions. For simplicity, we will restrict ourselves to the first harmonic of the Fourier series. In that case, Eq. (4) can be rewritten as

$$
\begin{aligned}
F(x) &= C \sum_{n=-1}^{n=1} A_n x^{\alpha + i\omega_n} \\
&= Cx^\alpha [A_0 + 2A_1 \cos(\omega \log x)],
\end{aligned}
\tag{5}
$$

where $A_1 = A_{-1}$ and $\omega = 2\pi/\log \lambda$. Due to the periodic term in $\log x$, discrete scale invariance is said to have a log-periodicity. Here ω is the angular frequency, which is determined by λ and has a unique value for a specific DSI. Since scale factors follow a geometric progression, DSI can represent hierarchical systems. Discrete scale invariance has

been observed in theoretical systems such as Cantor sets, hierarchical diamond lattices, and idealized Ising models [42,43]. Additionally, DSI has been found to exist in several heterogeneous and irreversible phenomena such as earthquakes and stock market crashes [15].

The presence of DSI in heterogeneous systems implies that critical phenomena can be viewed as hierarchical phenomena. For example, Sornette and Sammis [18] proposed that the occurrence of a large earthquake is a consequence of the propagation and accumulation of several preceding smaller earthquakes and ruptures in a large geographical area. Similar behavior has also been shown to precede stock market crashes. Johansen *et al.* [14] hypothesized that stock market crashes are caused by the slow buildup of long-range correlations leading to the collapse of the stock market in one critical instant. Thus, DSI provides additional constraints on a system (in terms of a preferred scale factor), eventually unraveling the underlying physical mechanism.

III. EXPERIMENTS

Experiments are performed on a turbulent combustor at high Reynolds numbers (Re > 14 000) with a circular bluff body as the flame-holding mechanism. A schematic diagram of the experimental setup is portrayed in Fig. 1(a). The system comprises a plenum or settling chamber and a combustion chamber with extension ducts. Fluctuations in the inlet air

are diminished in the plenum chamber. A circular disk with a radius of 47 mm and thickness of 10 mm is mounted on the central shaft as a bluff body. The fuel, liquefied petroleum gas (60% butane and 40% propane), is injected 100 mm upstream of the dump plane. The central shaft is used to deliver fuel into the combustor through four radial injection holes of diameter 1.7 mm in the central shaft.

The combustion chamber is cuboid in shape with a cross section of size 90×90 mm^2 and length 700 mm. A spark plug driven by a step-up transformer is mounted near the dump plane for ignition of the fuel-air mixture. Mass flow controllers (Alicat Scientific, MCR Series) are used to measure and control mass flow rates of air ($\dot{m}_a$) and fuel ($\dot{m}_f$) with an uncertainty of $\pm(0.8\%$ of the reading $+0.2\%$ of the full scale). The Reynolds number Re for the reactive flow is obtained as Re $= 4\dot{m}/\pi\mu(D_0 + D_1)$, where $\dot{m} = \dot{m}_a + \dot{m}_f$ is the mass flow rate of the air-flow mixture, D_0 is the diameter of the burner, D_1 is the diameter of the circular bluff body, and μ is the dynamic viscosity of the air-fuel mixture in the experimental conditions. The Reynolds number for the reported experiments is varied within a range from Re $= (1.41 \pm 0.08) \times 10^4$ to Re $= (5.3 \pm 0.26) \times 10^4$. We measure the acoustic pressure fluctuations in terms of voltage V using a piezoelectric sensor (PCB103B02, with sensitivity of 217.5 mV/kPa, resolution of 0.2 Pa, and uncertainty of 0.15 Pa) at a sampling rate of 12 kHz. The global heat release rate is measured from the CH* chemiluminescence intensity [45], which is captured using a photomultiplier tube (Hamamatsu H10722-01) outfitted with a bandpass filter (with a wavelength of 435 nm and a 10-nm full width at half maximum). More details of the experimental setup are discussed in [46].

In the present study, the global equivalence ratio ϕ [$\phi = \frac{(\dot{m}_f/\dot{m}_a)_{\text{actual}}}{(\dot{m}_f/\dot{m}_a)_{\text{stoichiometry}}}$] is decreased as we increase the air flow rate while keeping the fuel flow rate constant, at 1.07 g/s. The air flow rate (the control parameter) is varied linearly with respect to time t at a constant rate r. The equivalence ratio is varied from 1 to 0.25 continuously in time in each experiment. We perform experiments for different values of r ranging from 0.1 to 2.0 g/s^2. The variation of acoustic pressure over time, as we vary the airflow rate, is shown in Fig. 1(b) for $r = 0.6$ g/s^2. The blue (black) solid curve in the plot represents acoustic pressure fluctuations p' (in Pa), while the change of airflow rates is exhibited by the magenta (gray) solid curve. Initially, the thermoacoustic system is in a state of stable operation, and the amplitude of p' is close to 100 Pa. The amplitude of pressure fluctuations p' increases with the airflow rate ramping up at a constant rate r. The system experiences thermoacoustic instability due to positive feedback between the acoustic oscillations and the unsteady heat release rate [47]. The amplitude of p' reaches its maximum value during thermoacoustic instability. Further increments in airflow rates (i.e., reducing the equivalence ratio) result in the reduction of the amplitude of pressure fluctuations, and the combustor approaches blowout. The occurrence of blowout is determined as the instance at which heat release rate becomes zero and is represented by the red (gray) dashed line (T_c) in Fig. 1(b). In the rest of the paper, we focus on data close to blowout to serve our purposes.

IV. RESULTS

We observe from experiments the presence of low-frequency oscillations (approximately equal to 10 Hz) among other high-frequency fluctuations and aperiodicity, before the system goes to the blowout state. The appearance of low-frequency oscillations prior to blowout has been reported in the literature [5,48] and has been used to characterize blowout where control parameters were changed in a quasistatic manner. Here, in experiments with a continuously varying parameter, we also use those low-frequency oscillations to characterize blowout. As a result, we decompose p' into Fourier modes and construct a new time series from Fourier coefficients. Since we are varying the control parameter continuously, we perform the Fourier transform of p' window-wise. We consider 1-s windows with an overlap of 0.9 s to determine the amplitude spectrum at each time instance t_i (s). During this process, we identify a significant presence of a low-frequency spectrum with frequencies f from 5 to 25 Hz over the entire parameter range ($0.1 < r < 2.0$ g/s^2) explored in the present article. Therefore, in order to construct the desired time series, we define a new variable $A_f(t_i) = \max[C_f(f, t_i)]$, where $C_f(f, t_i)$ are Fourier coefficients of f for each t_i computed over the time window $[t_i - 1, t_i]$.

Blue (black) solid curves in Fig. 2 represent time series of A_f for different values r, the rate of change of airflow rate. Red dashed lines represent the blowout time T_c obtained from experiments. We determine T_c by measuring the global heat release rate. It is evident from those newly constructed time series that the value of A_f remains very small initially and starts to increase as blowout is approached. The rise in the value of A_f stops adjacent to blowout and experiences a rapid diminution after that. Such a behavior hints at a singularity in A_f accompanying a critical phenomenon, i.e., blowout. Note that the time at which the maximum of A_f occurs (T_m) and T_c may not coincide. However, they remain within a single time window chosen while deriving A_f. In other words, $|T_c - T_m| < 1$ s because we are dealing with a time window with a duration of 1 s. Thus, for all practical purposes, we consider T_c and T_m to be the same.

The system transitions to blowout earlier for a faster rate of change of airflow rates because the system reaches the critical equivalence ratio faster. However, the signature of the increment in A_f near blowout persists. The observed rise in A_f preceding blowout itself is an interesting phenomenon having a significant prognostic value. A similar behavior has been observed in the stock market index before the market crashes [17]. The rest of the discussion is based on the analysis of data segments plotted in Fig. 2.

A. Presence of oscillations preceding blowout in the time series data

First, we examine whether the A_f data preceding blowout possess log-periodic oscillations intrinsically. Towards this purpose, we perform a nonparametric test on A_f. The appearance of log-periodicity before blowout is determined following a method developed by Vandewalle *et al.* [49] to detect the log-periodic component preceding a market crash.
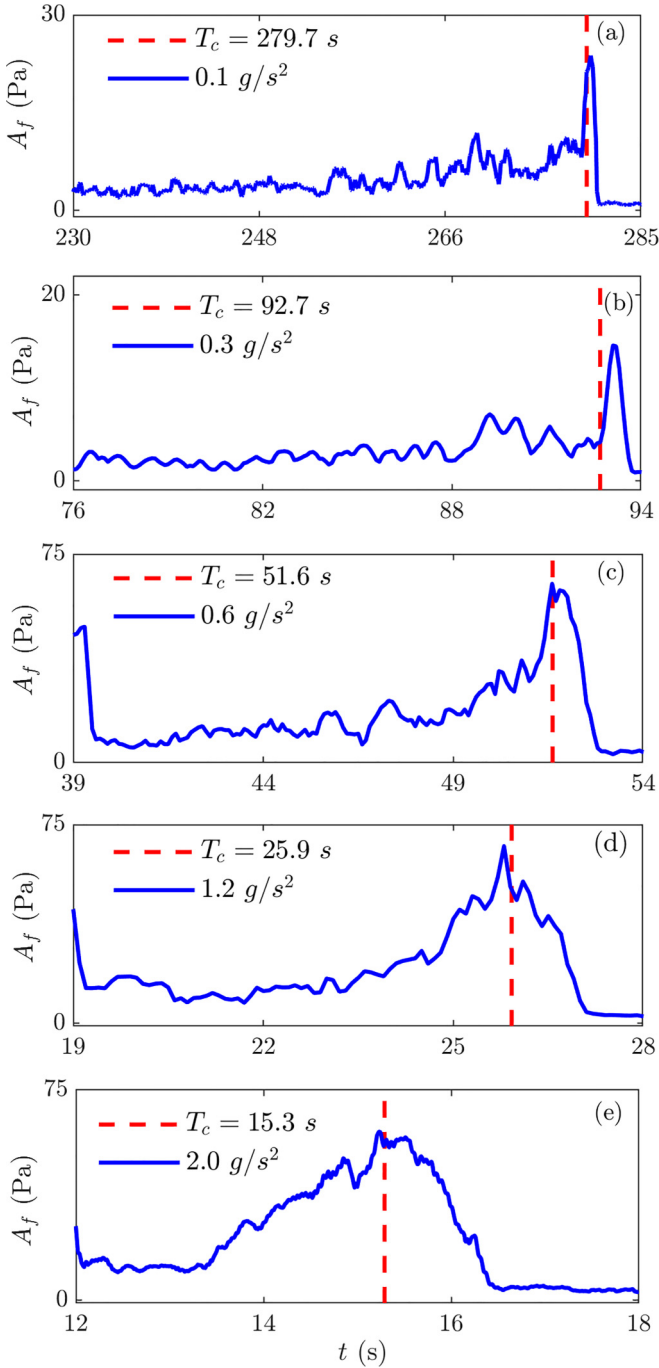
FIG. 2. Time series of the maximum of the amplitude spectrum A_f of low-frequency ($5 < f < 25$) [blue (black) solid curves] as obtained from experiments corresponding to different rates of change of the airflow rates. Red (dark gray) dashed lines represent the critical time T_c for blowout obtained from the heat release rate.

FIG. 3. Characteristics of log-periodic oscillations for rates of change of airflow rates (a), (c), and (e) 0.4 g/s² and (b), (d), and (f) 0.8 g/s² as obtained from experiments: (a) and (b) time series of A_f [blue (black) curves], (c) and (d) oscillations given by the difference between upper and lower envelope functions [red (dark gray) curves], and (e) and (f) the Lomb periodogram of log-periodic frequencies ω [green (dark gray) curves] of these oscillations.

In their method, log-periodic patterns are confirmed by computing the upper ($y_{\max}$) and lower ($y_{\min}$) envelope functions of the market index y. The upper envelope at any time t is the maximum of y until time t. Similarly, the lower envelope at t is the minimum of y from t to the end of the time series. The two envelopes never meet for a simple oscillation such as sinusoidal oscillation and their difference is constant. However, in the case of log-periodic power-law oscillations,
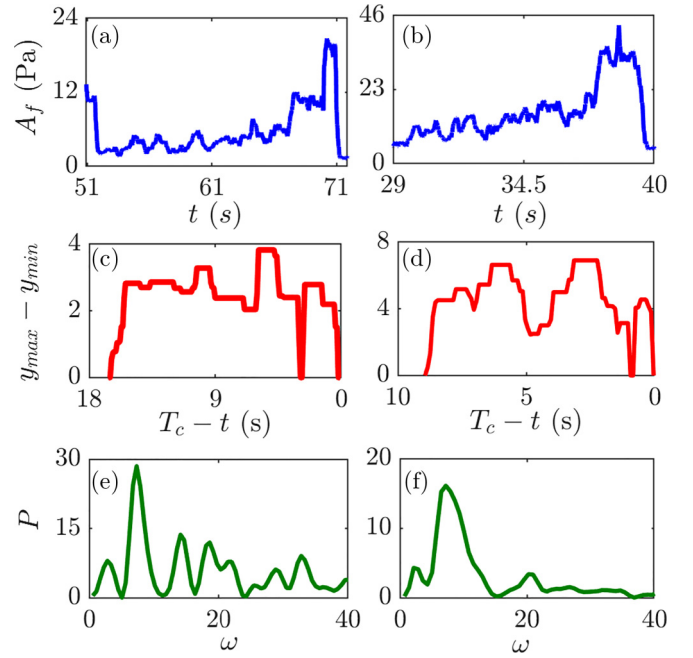
the two envelopes coincide at points where another period of oscillation begins and their difference becomes zero. Moreover, the appearance of such points increases as a system approaches a critical point following log-periodic oscillations. The two envelopes become equal because, at those points, they simultaneously attain a new value that they did not attain earlier. The difference between envelopes, also known as the running difference, comprises oscillations that correspond to log-periodic oscillations present in the time series. Vandewalle *et al.* [49] found that oscillations obtained in this way accelerate as the critical time of the crash is approached and fitted the log-periodic term $\cos[\omega \log(t_c - t)]$ to those oscillations. This method can highlight log-periodic oscillations.

In Fig. 3 we show the time series of A_f [Figs. 3(a) and 3(b)] for a rate of change of airflow rates 0.4 g/s² [Figs. 3(a), 3(c), and 3(e)] and 0.8 g/s² [Figs. 3(b), 3(d), and 3(f)]. Oscillations, as obtained from the running difference, are shown in Figs. 3(c) and 3(d). In Figs. 3(a) and 3(b), for the time series of A_f corresponding to the rate of change of airflow rates 0.4 and 0.8 g/s², oscillations are observed between 51 and 71 s and between 29 and 40 s, respectively. The frequency of oscillations obtained from the running difference increases as $t \to T_c$, which indicates the existence of log-periodicity in the time series of A_f prior to blowout. Note that here we treated the occurrence of the maximum of A_f as T_c to uncover the log-periodic oscillations. Next we perform a spectral analysis of the computed running difference in $\log(T_c - t)$ to assess the indicated log-periodicity. The spectral power P of the oscillatory components ω is shown in Figs. 3(e) and 3(f), whose

high peaks confirm the existence of log-periodic oscillations in thermoacoustic systems prior to blowout.

The computation of the running difference serves as a sufficient condition for detecting log-periodic oscillations. Therefore, in order to strengthen our claim of the presence of log-periodic oscillations in turbulent thermoacoustic systems prior to blowout, we will perform a power-law detrended measure of the time series of A_f. To serve this purpose, we need to remove an associated power-law trend from the time series to analyze the obtained residue. As a first step of the process, we will determine the power law associated with blowout. Note that the choice of a power law depends on how the observed variable evolves as the critical point T_c is approached. To understand the nature of power law and its exponents, we examine the growth rate of A_f in the next section.

B. Understanding the nature of the growth rate

To understand the growth of a system, we generally plot the time series of a system variable x in the log-linear or semilogarithmic scale ($\log x$ vs t). It is quite obvious that the differentiation of $\log(x)$ with respect to time t, i.e.,

$$\frac{d}{dt}\log(x) = \frac{1}{x}\frac{dx}{dt}, \tag{6}$$

provides the relative growth rate of x. We utilize semilogarithmic plots to retrieve this relative growth rate of x from slopes of the plotted time series without even knowing its explicit functional form. A constant slope indicates that the system grows exponentially. On the other hand, if the slope is increasing monotonically, the system is said to have a faster-than-exponential growth. A faster-than-exponential growth is accompanied by a singularity occurring at the critical time t_c [50]. Such growth can be represented by the equation

$$\frac{dx}{dt} = x^m, \quad m > 1, \tag{7}$$

yielding a solution of the form

$$x(t) = x(0)\left(1 - \frac{t}{t_c}\right)^{-1/(m-1)}. \tag{8}$$

Another way of quantifying the growth rate is to study the doubling time intervals $(\Delta t)_i$ over which the value of x doubles [51]. Mathematically, we can say that $x[t_n + (\Delta t)_n] = 2x_n$, where at the nth time t_n, $x_n = x(t_n)$. In the case of exponential growth of x, $(\Delta t)_i$ remains constant for all i. However, if x doubles faster over a short time, the nth time interval $(\Delta t)_n$ can be written as

$$(\Delta t)_n = 2^{-n(m-1)}(\Delta t)_0. \tag{9}$$

Then $(\Delta t)_n$ decreases following a geometric progression with the common factor $r = 2^{-(m-1)}$ (<1) and shrinks to zero as $t \to t_c$. Note that computing the doubling of x is not the only way to confirm a faster-than-exponential growth rate. In fact, this growth rate can be realized for any α times increment of x over a time interval $(\Delta t)_i$ with $\alpha > 1$. In that case, r can be generalized as

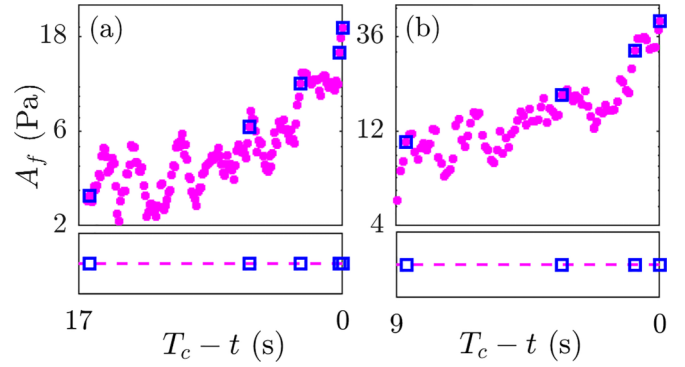$$r = \alpha^{-(m-1)}, \quad \alpha > 1, \quad m > 1. \tag{10}$$

FIG. 4. Semilogarithmic plots of A_f as a function of $T_c - t$ for rates of change of airflow rates (a) 0.4 and (b) 0.8 g/s². Open blue (black) squares plotted on the values of A_f [magenta (light gray) closed circles] represent successive α time increments of A_f values. Here T_c stands for the time at which the maximum of A_f occurs in experiments. In the bottom row, the projection of open blue (black) squares on the $A_f = 0$ [magenta (light gray) dashed] line shows the gradual diminution of time intervals which in turn quantifies a faster-than-exponential growth of A_f near blowout.

In the present work, we consider A_f as the system variable and set $\alpha = 1.25$ (1.35) for $r = 0.4$ g/s² (0.8 g/s²) portraying a 25% (35%) increment of A_f to inspect $(\Delta t)_i$.

In Fig. 4 we show the semilogarithmic plot of the part of the time series of A_f showing log-periodicity corresponding to different rates of change of airflow rates, 0.4 g/s² in Fig. 4(a) and 0.8 g/s² in Fig. 4(b). We estimate the growth function by calculating time intervals $(\Delta t)_i$ between each α time increment in the A_f value. Open blue (black) squares in Fig. 4 represent time instants forming $(\Delta t)_i$. We then project these time instances on the line corresponding to $A_f = 0$ [pink (light gray) dashed line shown in the bottom panel of Fig 4] to reveal the fact that, for a fixed rate of change of airflow rate, time intervals $(\Delta t)_i$ gradually decrease as the system approaches blowout. Consequently, A_f achieves a higher value in a short range of time close to blowout and becomes singular there. In each of these cases, it is apparent from the plot that the slope of $\log(A_f)$ is not a constant but changes as t approaches the critical time to blowout T_c. Therefore, based on the above discussion, we approximate A_f as

$$A_f \approx (t_c - t)^{-1/(m-1)}, \tag{11}$$

where t_c denotes an approximated value of the experimentally obtained blowout time T_c. Earlier, Johansen and Sornette [52] showed that the accelerated growth rate of an observable, such as the world population, gross domestic product of the world, and financial indices, can be approximated by a similar power law, leading to a superexponential behavior. Interestingly, the faster-than-exponential growth has also been realized in the spread of Covid-19 during the occurrence of the devastating Delta wave [53].

Based on the approximation given by Eq. (11), we adopt a generalized power-law representation for A_f as

$$y(t) = A + B(t_c - t)^{-1/(m-1)}, \tag{12}$$

where A and B are the linear parameters and t_c and m are the nonlinear parameters. The variable y and the parameter t_c in
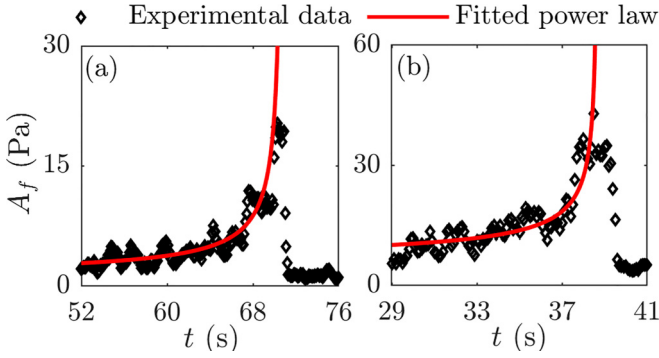
FIG. 5. Power-law fits to A_f corresponding to rates of change of airflow rates (a) 0.4 and (b) 0.8 g/s^2. Black markers represent A_f obtained from the experiment. The red (dark gray) curve represents Eq. (12) fitted to A_f. As $t \to t_c$, the fitted curve grows to infinity. The obtained parameter values are (a) $t_c = 70.8$ and $m = 2.28$ and (b) $t_c = 38.7$ and $m = 2.86$. The R^2 values for the power-law fit are (a) 0.54 and (b) 0.55.

Eq. (12) approximates A_f and T_c, respectively. In the rest of the discussion, by t_c we refer to the predicted time for blowout (T_c) obtained by curve fitting.

Next we fit Eq. (12) to the time series of A_f for different values of r. In Fig. 5 we fit Eq. (12) to A_f for rates of change airflow rates 0.4 g/s^2 [Fig. 5(a)] and 0.8 g/s^2 [Fig. 5(b)]. A power-law fit gives $t_c = 70.8$ and 38.7 s for $r = 0.4$ and 0.8 g/s^2, respectively. Since our purpose here is to identify the underlying log-periodicity, we choose the set of parameters such that the t_c remain very close to the actual time of occurrence of blowout. It is quite apparent from Fig. 5 that A_f values show oscillations with respect to the power-law curve, which could be log-periodic oscillations. In the next section, we discuss these oscillations in detail.

C. Confirmation of log-periodic oscillations

A parametric detrended analysis given by Johansen *et al.* [14] can also detect log-periodic oscillations. We use this method to confirm qualitatively the presence of log-periodic oscillations already detected by the nonparametric method (discussed in Sec. II) in the time series of A_f. To serve that purpose, we first subtract the parameter A in Eq. (12) from the actual A_f data. Then we detrend the power law $(t_c - t)^{-1/(m-1)}$ from this subtracted time series and perform Lomb periodogram analysis of the obtained residue s in $\log(t_c - t)$. The residue is given as

$$s(t) = (A_f - A)/(t_c - t)^{-1/(m-1)}, \quad (13)$$

with A, m, and t_c discussed in the preceding section. Here μ and σ are the mean and the standard deviation of s. Plotted in Fig. 6(a) is the normalized s with $\log(t_c - t)$, which shows some coarse oscillations. The power spectral density of the residue s is shown in Fig. 6(b). Here $\omega = 2\pi f$ is the log-angular frequency conjugate to $\log(t_c - t)$.

From Fig. 6(b) we find that higher peaks in both cases occur when $\omega < 50$. Hence, we interpret $\omega = 50$ as an upper limit for detecting fundamental log-periodic frequency.

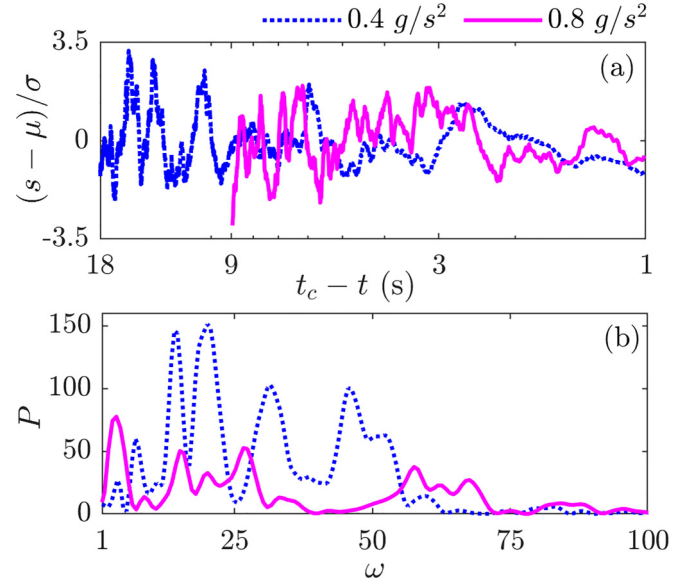Now, from the above discussion, it is evident that the preceding analysis confirms the presence of log-periodic

FIG. 6. (a) Power-law detrended oscillations for rates of change of airflow rates 0.4 g/s^2 [blue (black) dotted curve] and 0.8 g/s^2 [magenta (gray) solid curve]. Normalized s are plotted as a function of $\log(t_c - t)$ to get log-periodic oscillations. (b) Lomb spectral power of log-periodic frequencies.

oscillations prior to blowout in the A_f data corresponding to different rates of change of airflow rates. These log-periodic oscillations confirm the presence of discrete scale invariance in thermoacoustic systems en route to blowout.

D. Log-periodic power-law fitting

Equation (12) with log-periodic correction [21] is given as

$$y(t) = A + B(t_c - t)^{-1/(m-1)}$$
$$+ C(t_c - t)^{-1/(m-1)} \cos[\omega \log(t_c - t) - \tau], \quad (14)$$

where ω and τ are the angular frequency and the phase of the log-periodic oscillations. Equation (14) consists of seven parameters, out of which three are linear and four are nonlinear. The linear parameters are A, B, and C and the nonlinear parameters are t_c, m, ω, and τ. Due to the presence of a high number of nonlinear parameters, there are ambiguities in determining the parameters appropriately. Filiminov and Sornette [54] proposed a simplification of Eq. (14) by incorporating the effect of τ into linear parameters and introduced two new parameters $C_1 = C \cos(\tau)$ and $C_2 = C \sin(\tau)$ instead of C and τ. In the present study, we follow the modified log-periodic equation proposed by Filiminov and Sornette [54] given by

$$y(t) = A + B(t_c - t)^{-1/(m-1)}$$
$$+ (t_c - t)^{-1/(m-1)}\{C_1 \cos[\omega \log(t_c - t)]$$
$$+ C_2 \sin[\omega \log(t_c - t)]\}. \quad (15)$$

This form of log-periodic equation (15) has four linear parameters, namely, A, B, C_1, and C_2, and three nonlinear parameters t_c, m, and ω. The parameters are determined by minimizing
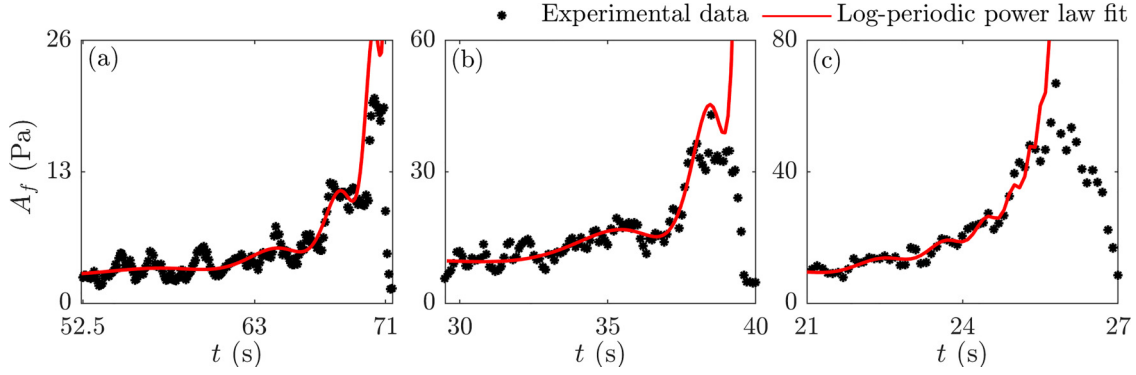
FIG. 7. Log-periodic power-law fit [red (gray) solid curves] to the experimentally obtained A_f data (black markers) for different rates of change of airflow rates: (a) 0.4 g/s^2, (b) 0.8 g/s^2, and (c) 1.2 g/s^2. The nonlinear parameter values for these curves are (a) $t_c = 72.6$, $m = 1.6$, and $\omega = 10.02$; (b) $t_c = 40.4$, $m = 1.67$, and $\omega = 7.67$; and (c) $t_c = 25.9$, $m = 2.54$, and $\omega = 14.5$. The R^2 values of the log-periodic power-law fit are (a) 0.62, (b) 0.58, and (c) 0.72.

the cost function

$$z = \sum_{i=1}^{N} (p_i - y_i)^2 \qquad (16)$$

over a time interval $[t_1, t_2]$ containing N data points, where $p_i = A_f(t_i)$ is the value of data at the ith time t_i and $y_i = y(t_i)$ is obtained from Eq. (15). Among these seven parameters involved in the cost function, the linear and nonlinear parameters are solved separately. Initially, linear parameters, namely, A, B, C_1, and C_2, are determined uniquely in terms of the nonlinear parameters by equating the first-order partial derivatives of the cost function z with respect to linear parameters to zero. Now z becomes a function of nonlinear parameters only. Then t_c, m, and ω are determined using the nonlinear least-squares method, the Nelder-Mead simplex method [55]. The characteristics of all seven parameters are discussed in the Appendix.

In Fig. 7 we fit Eq. (15) to the A_f data for three different rates of change of airflow rates r, 0.4 g/s^2 [Fig. 7(a)], 0.8 g/s^2 [Fig. 7(b)], and 1.2 g/s^2 [Fig. 7(c)]. The fitted curves are shown in red (gray), while black markers represent data points obtained from the experiment. The predicted times for blowout or t_c are 72.6 s [Fig. 7(a)], 40.4 s [Fig. 7(b)], and 25.9 s [Fig. 7(c)]. The final point of the time interval t_2 selected for computation is 1 s earlier than T_c in each case. As the system approaches blowout, the fitted curve (shown in red) starts to grow and diverges. We also fit Eq. (15) to

several other data sets for different values of r. A comparison between the mean of predicted blowout times t_c given by the pure power law (11), the LPPL (15), and the actual blowout time T_c for different values of the parameter r are given in Table I. Here the mean of t_c is the mean of 100 optimum t_c. The selection of these optimum values of t_c is discussed in the Appendix. We can clearly observe from Table I that predictions made by the LPPL are better than the pure power law. Moreover, we calculate errors ($e = |t_c - T_c|$) for t_c given by the LPPL formulation for different values of r, which are shown in the last column of Table I.

The wobbles in the LPPL curve in Fig. 7 are due to log-periodic oscillations. The local maxima or peaks of the curve are related to the underlying discrete scale-invariance property. Therefore, it is desirable that the predicted A_f (or y) at those peaks are correlated to each other and may be associated with some hierarchical structure or collective behavior of microscopic components of the system, which ceases to exist as blowout occurs.

Note that the solution to the nonlinear parameters eventually gives the predicted time for critical phenomena t_c, which corresponds to the time of blowout in the present case. Therefore, it will be interesting to know how early and how accurately we can predict blowout using Eq. (15), which we will discuss in the next section.

E. Early prediction of blowout

Although t_c is the predicted time of blowout, it is more reliable to consider the mean of t_c for robust and accurate predictions instead of any particular instances of it. To serve this purpose, we first generate 5×10^4 realizations of t_c, m, and ω for a sample space over the time window $[t_1, t_2]$. Then we determine the 95% confidence interval of t_c. We repeat the procedure for different sample spaces from a particular data set over $[t_1, t_2]$ by varying t_2. In Fig. 8 we have plotted the predicted time of blowout t_c together with error bars [blue (gray) markers] as a function of $T_c - t_2$ for airflow rates of 0.4 and 0.8 g/s^2. The absolute value of $T_c - t_2$ signifies how far the actual onset of blowout is from the present state of the system, i.e., the precedence of prediction. The region shaded in cyan (light gray) signifies a precision region of T_c [red (gray)

TABLE I. Experimentally determined and mean of the predicted critical time for blowout for different rates of change of airflow rates. The predictions made by the LPPL are better than those by the power law.

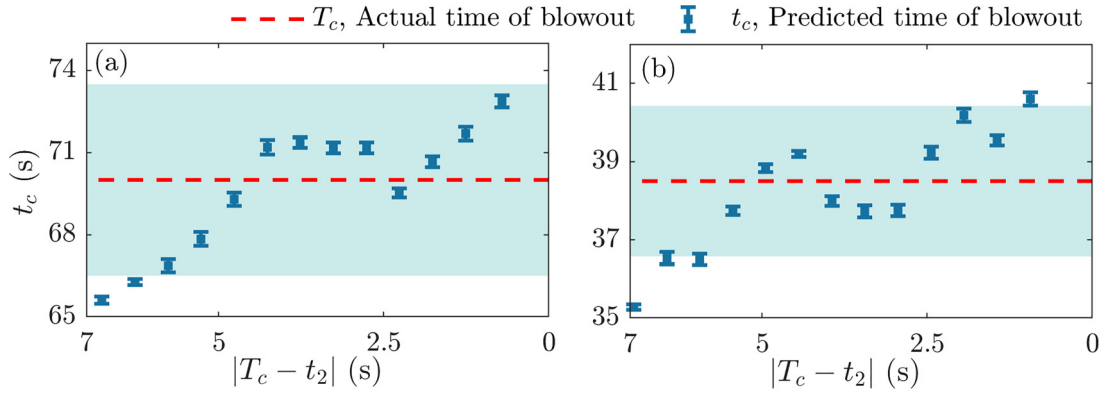| r (g/s^2)	t_c (s), power law	t_c (s), LPPL	T_c (s), LBO	e (s), LPPL
0.1	288.5	284.7	279.7	5.0
0.4	75.5	72.9	70.0	2.9
0.8	43.3	40.6	38.5	0.9
1.2	29.2	26.2	25.9	0.3
2.0	16.3	16.2	15.3	0.9

FIG. 8. Predicted time to blowout t_c with error bars [blue (black) markers] plotted with respect to $T_c - t_2$ for different rates of change of airflow rates: (a) 0.4 g/s^2 and (b) 0.8 g/s^2. The red (dark gray) dashed line represents the experimentally obtained blowout time T_c. The cyan-shaded region represents a threshold region of T_c.

dashed line] having a 5% relaxation. If a t_c, or its error bar, intersects the precision region, we can say that the associated interval ending at t_2 predicts T_c well. In Fig. 8(a), predictions together with their error remain within the precision region for $T_c - t_2 \leqslant 6$ s. In other words, better prediction can be given up to 6 s earlier than the actual occurrence of blowout; after that, the predicted t_c deviates from T_c. Similarly, in the case of rate of change of an airflow rate of 0.8 g/s^2 [Fig. 8(b)], we can approximate blowout up to 6.5 s earlier. Thus, the LPPL model, given by Eq. (14), can approximate the occurrence of blowout quite well. However, to fit the LPPL, we need enough data consisting of at least one or two oscillations. Hence, the prediction could potentially fail for very fast rates of variation of control parameters. Since blowout occurs early with the increment of the rate of change of airflow rates, the distance between t_1, the starting point of the time interval over which fitting is performed, and t_c decreases. Consequently, data points in the interval $[t_1, t_2]$ also decrease and become sparse for faster rates. When there is not enough data, predictions become challenging.

V. CONCLUSION

In this work we characterized the dynamics of a thermoacoustic system close to lean blowout. We investigated the temporal variation of the maximum of coefficients of low-frequency spectrum with frequencies f from 5 to 25 Hz, denoted by A_f. The A_f was computed from pressure fluctuations p' obtained from a laboratory-scale turbulent combustor for different rates of change of the control parameter. We showed that the occurrence of blowout, from the perspective of statistical physics, bears the signatures of a critical point. The value of A_f after a specific time starts to increase with an oscillation of increasing frequency and continues until blowout. Thus, A_f attains a finite-time singularity at the critical time where blowout occurs. We discovered that such an oscillation in A_f prior to blowout is the so-called log-periodic oscillation. The presence of a log-periodic power law indicates an underlying discrete scale invariance. Thus, we speculated that blowout can occur as a hierarchical phenomenon. Blowout has already been interpreted as the extinction of flames by the formation of global flame holes [5,7,9]. The formation of local flame holes causes local flame extinction followed by reignition. The number and the frequency of extinction and reignition events increase as the system approaches blowout. Each extinction is a part of the precursory sequence of an even larger event with more local flame holes during such a progression. At the critical time when blowout occurs, the collective behavior of local flame holes leads to the formation of a large flame hole that ultimately results in blowout. Therefore, the formation of such global flame holes can be considered a scaling-up
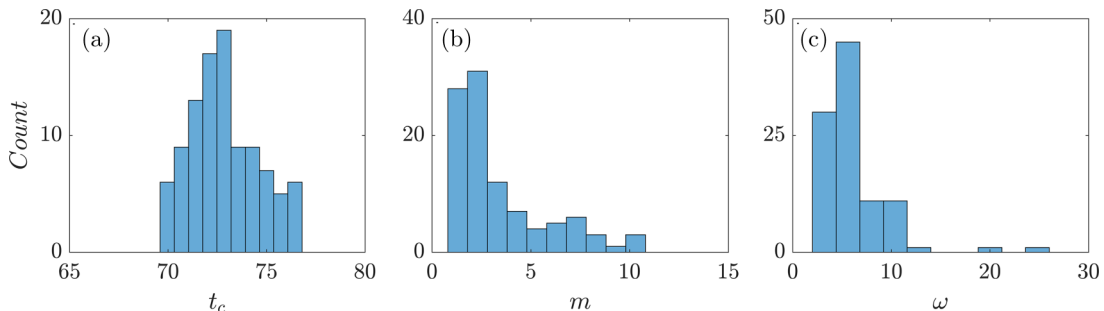

FIG. 9. Histogram of nonlinear parameters (a) t_c, (b) m, and (c) ω [blue (gray) bars], computed over 100 realizations for rates of change of airflow rate 0.4 g/s^2. The number of counts in each bin for each parameter is along vertical axis.

process where each local extinction event is associated with intermediate scales in a geometric progression. However, further investigations are required to confirm the origin of log-periodicity close to blowout in thermoacoustic systems.

We also noticed that the growth of the amplitude of A_f in the close vicinity of blowout follows a faster-than-exponential scaling law. Such a scaling law decorated with log-periodic oscillations gives a deterministic model to characterize A_f prior to an impending blowout. Using the model, we were able to predict the occurrence of blowout well in advance for different rates of change of airflow rates. Note that power law can also be used to predict the time of blowout. However, far away from the critical point, the fitting using log-periodicity gives a better prediction compared to the power law. Therefore, we expect that the model derived in the present work can serve the purpose of predicting impending blowout in lean operating combustors, enabling us to take control of the action in time to evade it.

ACKNOWLEDGMENTS

APPENDIX

The log-periodic model given by Eq. (15) is calibrated on the data within a time interval $[t_1, t_2]$. In the present analysis, we keep t_1 fixed and vary t_2. In order to determine the parameters, we start with a random initial guess of the nonlinear parameters t_c, m, and ω. First, the linear parameters are determined uniquely by minimizing the cost function z from Eq. (16) with respect to the linear parameters. In other
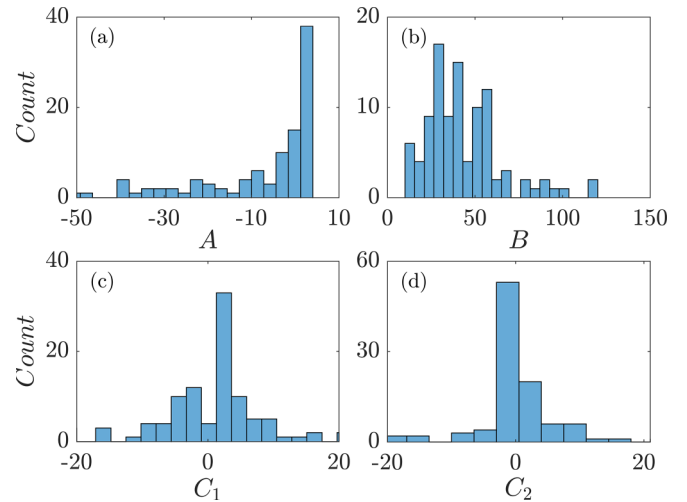

FIG. 10. Histogram of linear parameters (a) A, (b) B, (c) C_1, and (d) C_2 [blue (gray) bars] for rates of change of airflow rate 0.4 g/s^2. Ordinates represent the number of counts in each bin for each parameter.

words, the equation

$$\frac{\partial z}{\partial X} = 0, \qquad (A1)$$

where $X = A$, B, C_1, and C_2, are solved to get A, B, C_1, and C_2. Then we determine nonlinear parameters using the nonlinear least-squares method. We use a MATLAB-based package FMINSEARCH to determine t_c, m, and ω. We perform 100 realizations for each time interval examined in the present analysis. To increase the robustness of the process of determining parameters, each of the realizations consists of 500 iterations. We then compute the sum-squared error (SSE) for all 500 iterations. The best set of parameters is considered to be associated with a minimum SSE for each realization. Histograms of 100 such best sets of parameter values are shown in Figs. 9 and 10 for a rate of change of airflow rate of 0.4 g/s^2. The histograms depict the fact that although the initial values of the nonlinear parameters are randomly selected, the computed final values are not scattered widely from their mean.

[1] S. R. Turns, *Introduction to Combustion* (McGraw-Hill, New York, 1996), Vol. 287.

[2] T. C. Lieuwen, *Unsteady Combustor Physics* (Cambridge University Press, Cambridge, 2021).

[3] S. Plee and A. Mellor, Characteristic time correlation for lean blowoff of bluff-body-stabilized flames, Combust. Flame **35**, 61 (1979).

[4] K. Radhakrishnan, J. B. Heywood, and R. J. Tabaczynski, Premixed turbulent flame blowoff velocity correlation based on coherent structures in turbulent flows, Combust. Flame **42**, 19 (1981).

[5] S. Nair and T. Lieuwen, Acoustic detection of blowout in premixed flames, J. Propul. Power **21**, 32 (2005).

[6] S. Nair, Acoustic characterization of flame blowout phenomenon, Ph.D. thesis, Georgia Institute of Technology, 2006, https://www.proquest.com/pagepdf/305333220?accountid=170785.

[7] S. Nair and T. Lieuwen, Near-blowoff dynamics of a bluff-body stabilized flame, J. Propul. Power **23**, 421 (2007).

[8] S. Chaudhuri and B. M. Cetegen, Blowoff characteristics of bluff-body stabilized conical premixed flames with upstream spatial mixture gradients and velocity oscillations, Combust. Flame **153**, 616 (2008).

[9] S. Chaudhuri, S. Kostka, M. W. Renfro, and B. M. Cetegen, Blowoff dynamics of bluff body stabilized turbulent premixed flames, Combust. Flame **157**, 790 (2010).

[10] T. M. Muruganandam and J. M. Seitzman, Fluid mechanics of lean blowout precursors in gas turbine combustors, Int. J. Spray Combust. Dyn. **4**, 29 (2012).

[11] V. R. Unni, S. Chaudhuri, and R. I. Sujith, Flame blowout: Transition to an absorbing phase, Chaos **28**, 113121 (2018).

[12] T. Muruganandam, S. Nair, D. Scarborough, Y. Neumeier, J. Jagoda, T. Lieuwen, J. Seitzman, and B. Zinn, Active control of lean blowout for turbine engine combustors, J. Propul. Power **21**, 807 (2005).

[13] D. Sornette, P. Miltenberger, and C. Vanneste, Statistical physics of fault patterns self-organized by repeated earthquakes, Pure Appl. Geophys. **142**, 491 (1994).

[14] A. Johansen, O. Ledoit, and D. Sornette, Crashes as critical points, Int. J. Theor. Appl. Finance **03**, 219 (2000).

[15] D. Sornette, Discrete-scale invariance and complex dimensions, Phys. Rep. **297**, 239 (1998).

[16] H. Saleur, C. G. Sammis, and D. Sornette, Discrete scale invariance, complex fractal dimensions, and log-periodic fluctuations in seismicity, J. Geophys. Res.: Sol. Ea. **101**, 17661 (1996).

[17] D. Sornette, *Why Stock Markets Crash* (Princeton University Press, Princeton, 2009).

[18] D. Sornette and C. G. Sammis, Complex critical exponents from renormalization group theory of earthquakes: Implications for earthquake predictions, J. Phys. (France) I **5**, 607 (1995).

[19] J. Faillettaz, A. Pralong, M. Funk, and N. Deichmann, Evidence of log-periodic oscillations and increasing icequake activity during the breaking-off of large ice masses, J. Glaciol. **54**, 725 (2008).

[20] J.-C. Anifrani, C. Le Floc'h, D. Sornette, and B. Souillard, Universal log-periodic correction to renormalization group scaling for rupture stress prediction from acoustic emissions, J. Phys. (France) I **5**, 631 (1995).

[21] D. Sornette, A. Johansen, and J.-P. Bouchaud, Stock market crashes, precursors and replicas, J. Phys. (France) I **6**, 167 (1996).

[22] J. H. Wosnitza and D. Sornette, Analysis of log-periodic power law singularity patterns in time series related to credit risk, Eur. Phys. J. B **88**, 97 (2015).

[23] G. Sturgess and D. Shouse, *Turbo Expo: Power for Land, Sea, and Air* (American Society of Mechanical Engineers, New York, 1993), Vol. 78910, p. V03BT16A088.

[24] E. Ahmed and Y. Huang, Hybrid lean blowout prediction methodology with reactive flow simulation, Combust. Sci. Technol. **189**, 1776 (2017).

[25] Y. Wang and W. Song, Experimental investigation of influence factors on flame holding in a supersonic combustor, Aerosp. Sci. Technol. **85**, 180 (2019).

[26] S. H. Strogatz, *Nonlinear Dynamics and Chaos with Student Solutions Manual: With Applications to Physics, Biology, Chemistry, and Engineering* (CRC, Boca Raton, 2018).

[27] Y. Bar-Yam, S. R. McKay, and W. Christian, Dynamics of complex systems (studies in nonlinearity), Comput. Phys. **12**, 335 (1998).

[28] R. Hoyle and R. B. Hoyle, *Pattern Formation: An Introduction to Methods* (Cambridge University Press, Cambridge, 2006).

[29] H. Gotoda, H. Nikimoto, T. Miyano, and S. Tachibana, Dynamic properties of combustion instability in a lean premixed gas-turbine combustor, Chaos **21**, 013124 (2011).

[30] H. Gotoda, M. Amano, T. Miyano, T. Ikawa, K. Maki, and S. Tachibana, Characterization of complexities in combustion instability in a lean premixed gas-turbine model combustor, Chaos **22**, 043128 (2012).

[31] H. Gotoda, Y. Shinoda, M. Kobayashi, Y. Okuno, and S. Tachibana, Detection and control of combustion instability based on the concept of dynamical system theory, Phys. Rev. E **89**, 022910 (2014).

[32] A. Mukhopadhyay, R. R. Chaudhari, T. Paul, S. Sen, and A. Ray, Lean blow-out prediction in gas turbine combustors using symbolic time series analysis, J. Propul. Power **29**, 950 (2013).

[33] V. Nair and R. I. Sujith, Multifractality in combustion noise: Predicting an impending combustion instability, J. Fluid Mech. **747**, 635 (2014).

[34] V. R. Unni and R. I. Sujith, Multifractal characteristics of combustor dynamics close to lean blowout, J. Fluid Mech. **784**, 30 (2015).

[35] V. R. Unni and R. I. Sujith, in *Proceedings of the 52nd AIAA/SAE/ASEE Joint Propulsion Conference, Salt Lake City, 2016* (AIAA, Reston, 2016), paper 2016-4649.

[36] S. De, A. Bhattacharya, S. Mondal, A. Mukhopadhyay, and S. Sen, Application of recurrence quantification analysis for early detection of lean blowout in a swirl-stabilized dump combustor, Chaos **30**, 043115 (2020).

[37] C. Bhattacharya, S. De, A. Mukhopadhyay, S. Sen, and A. Ray, Detection and classification of lean blow-out and thermoacoustic instability in turbulent combustors, Appl. Therm. Eng. **180**, 115808 (2020).

[38] S. J. Shanbhogue, S. Husain, and T. Lieuwen, Lean blowoff of bluff body stabilized flames: Scaling and dynamics, Prog. Energy Combust. Sci. **35**, 98 (2009).

[39] R. I. Sujith and V. R. Unni, Dynamical systems and complex systems theory to study unsteady combustion, Proc. Combust. Inst. **38**, 3445 (2021).

[40] B. B. Mandelbrot and B. B. Mandelbrot, *The Fractal Geometry of Nature* (Freeman, New York, 1982), Vol. 1.

[41] P. Bak, *How Nature Works: The Science of Self-Organized Criticality* (Springer Science + Business Media, New York, 2013).

[42] B. Derrida, L. De Seze, and C. Itzykson, Fractal structure of zeros in hierarchical models, J. Stat. Phys. **33**, 559 (1983).

[43] Y. Meurice, G. Ordaz, and V. G. J. Rodgers, Evidence for Complex Subleading Exponents from the High-Temperature Expansion of Dyson's Hierarchical Ising Model, Phys. Rev. Lett. **75**, 4555 (1995).

[44] T. Komarek and W. Polifke, Impact of swirl fluctuations on the flame response of a perfectly premixed swirl burner, J. Eng. Gas Turbines Power **132**, 061503 (2010).

[45] Y. Hardalupas and M. Orain, Local measurements of the time-dependent heat release rate and equivalence ratio using chemiluminescent emission from a flame, Combust. Flame **139**, 188 (2004).

[46] M. Raghunathan, N. B. George, V. R. Unni, P. R. Midhun, K. V. Reeja, and R. I. Sujith, Multifractal analysis of flame dynamics during transition to thermoacoustic instability in a turbulent combustor, J. Fluid Mech. **888**, A14 (2020).

[47] M. P. Juniper and R. I. Sujith, Sensitivity and nonlinearity of thermoacoustic oscillations, Annu. Rev. Fluid Mech. **50**, 661 (2018).

[48] T. Yi and E. J. Gutmark, Real-time prediction of incipient lean blowout in gas turbine combustors, AIAA J. **45**, 1734 (2007).

[49] N. Vandewalle, M. Ausloos, P. Boveroux, and A. Minguet, Visualizing the log-periodic pattern before crashes, Eur. Phys. J. B **9**, 355 (1999).

[50] D. Sornette and J. V. Andersen, A nonlinear super-exponential rational model of speculative financial bubbles, Int. J. Mod. Phys. C **13**, 171 (2002).

[51] C. G. Sammis and D. Sornette, Positive feedback, memory, and the predictability of earthquakes, Proc. Natl. Acad. Sci. USA **99**, 2501 (2002).

[52] A. Johansen and D. Sornette, Finite-time singularity in the dynamics of the world population, economic and financial indices, Physica A **294**, 465 (2001).

[53] I. Pavithran and R. I. Sujith, Extreme COVID-19 waves reveal hyperexponential growth and finite-time singularity, Chaos **32**, 041104 (2022).

[54] V. Filimonov and D. Sornette, A stable and robust calibration scheme of the log-periodic power law model, Physica A **392**, 3698 (2013).

[55] J. A. Nelder and R. Mead, A simplex method for function minimization, Comput. J. **7**, 308 (1965).